Modelling and Stability Control of Two-Wheeled Robots in Low-Traction Environments

Daniel R. Jones and Karl A. Stol
Department of Mechanical Engineering
University of Auckland, New Zealand
danielrjones1@gmail.com, k.stol@auckland.ac.nz

Abstract

Much research on two-wheeled robots has been completed in the past decade, but robot stability in low-traction environments has not yet been considered. A model for the two-wheeled robot including wheel slip effects is derived. A wheel slip dependent friction model is used to simulate two low-traction surfaces: the first has characteristics similar to ice and the second is frictionless, in addition to a no-slip environment.

Two reference-tracking controllers designed for low-traction surfaces are described, and their effect on robot stability is compared to a typical controller designed for no-slip surfaces. The control objective of robot stability is tested by observing the tilt angle response of the robot, starting at rest with an initial tilt angle of 10°. In simulations only the two new controllers are able to maintain robot stability on frictionless surfaces, and both outperform the baseline controller on other surfaces. A controller is used experimentally to achieve robot balance in the presence of mass imbalances and tilt angle measurement errors, using a reaction wheel actuator on a frictionless surface, but the controller is unable to balance on no-slip surfaces due to unmodelled tire effects.

1 Introduction

Mobile robotics is a rapidly expanding field. In the near future, mobile robots could be used in a large number of applications, particularly in assisting and interacting with humans e.g. transporting materials around offices or hospitals, domestic activities, etc.

One mobile robot configuration is the two wheeled robot (TWR). This configuration consists of two drive wheels mounted along a single axis of the intermediate body (IB) which houses the system hardware. TWRs have a number of advantages over other configurations, including mechanical simplicity, zero-radius turning which allows navigation through confined spaces, and superior stablility on steep inclines (by leaning forward into the incline).

A TWR is a dynamically unstable system, requiring a controller to maintain balance. A large amount of research on this topic has been completed [Grasser *et al.*, 2002; Kim *et al.*, 2005; Shimada and Hatakeyama, 2008]. Robot stability has been achieved with both full-state feedback and reference-tracking controllers, therefore a similar controller will be used as the baseline in this study.

It is apparent, however, that all researchers in this field have assumed there will be no slip between the drive wheels and the ground. In environments with sufficient tire-ground traction, this assumption is satisfied; however, in other environments such as loose sand, wet grass or ice, such controllers will quickly lose balance. Nguyen et al. [2004] list this as one weakness of the Segway RMP. In applications involving interaction with humans, a loss of balance could be disastrous. Therefore existing TWR controllers are limited to areas with sufficient tire-ground traction, or require special tires to extend their operating envelope; these special tires have been found to decrease battery life [Nguyen *et al.*, 2004].

The aim of low-traction research is to address this limitation by developing an improved controller which models and accounts for wheel slip, and also to test the effectiveness of an additional actuator beyond the two drive wheels. The additional actuator of interest is an inertia- or reaction-wheel mounted along an axis parallel to the drive wheel axle. When accelerated, the reaction-wheel exerts a reaction torque on the IB which can be used by the controller to achieve balance.

The mobile robot will be restricted to longitudinal motion in a two dimensional plane, i.e. the robot is able to alter pitch and move forwards and backwards, but yaw changes will not be considered. Additionally, only flat, non-deformable types of terrain will be considered e.g. lubricated asphalt, wet concrete, ice etc. This simplifies

the system by eliminating movement in the vertical direction and ensuring the effects of rolling resistance are negligible. Parallel efforts at the University of Auckland focus on TWR control in uneven terrain [Kausar *et al.*, 2010].

1.1 Tire-Terrain Traction Research

The vast majority of models for traction between a rolling tire and the terrain surface assume that the longitudinal traction force is proportional to the normal force and is related by the coefficient of friction, μ, which must be determined experimentally for each surface combination.

Under classical friction theory, or Coulomb friction, the coefficient of friction can take one of two values, either the static or kinetic coefficient. A number of researchers have found that the tire-terrain friction coefficient is better modelled as a function of wheel slip, s [Pacejka *et al.*, 1987; Wong, 1978]

$$s = \frac{\omega r - v}{max(\omega r, v)} \tag{1}$$

where ω is the angular velocity of the wheel, r is the wheel radius, and v is the linear velocity of the wheel axle. Ward and Iagnemma [2008] proposed a non-normalised replacement for wheel slip, the relative velocity: $v_r = \omega r - v$. Using this quantity rather than wheel slip as the basis for the friction model eliminates the singularity at zero velocities. Additionally, it is expected that most TWR applications will have relatively small wheel velocities, so normalisation is unnecessary. For these reasons, the relative wheel velocity is used.

Figure 1 shows a collection of idealised friction coefficient curves for various surfaces and wheel slip values. Note that wheel slip is illustrated rather than relative wheel velocity. However, the curve shapes are very similar in both cases. At small values of wheel slip, the friction coefficient rises linearly, before reaching a critical peak value; past this critical point, the force distribution in the tire breaks down and the wheel begins to slip, resulting in a decreasing friction coefficient. The curve shapes vary depending on a plethora of factors, including tire characteristics (compound, tread depth, pressure, etc.), road conditions (texture, drainage, lubricant, etc.) and vehicle operational conditions (load, velocity).

Many researchers have attempted to fit formulae to the wheel slip-friction coefficient curve, to aid with modelling and estimation. The most popular formula is Pacejka's "Magic Formula" [1987] which utilises six parameters to fit a wheel slip curve. Pacejka's formula can be fit to many different traction scenarios with high accuracy. However, Ward and Iagnemma [2008] identified one disadvantage of this formula to be the number of parameters required. They proposed a different formulation which only requires three fitting parameters to overcome this

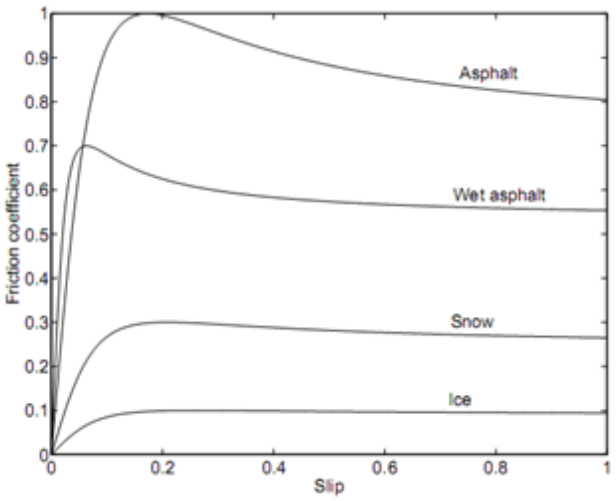

Figure 1: Friction coefficient versus wheel slip curves for various surfaces, with exaggerated initial slope, reproduced from [Gustafsson, 1997]

limitation, with reasonable accuracy close to zero relative wheel velocity. However, wheel slip curves produced by this formula do not plateau at large relative wheel velocities, which was found to cause simulation errors. Consequently, a modified formula, Equation (2), was used in this research.

$$\mu(v_r) = sign(v_r)\Big[C_1(1 - e^{-A_1\|v_r\|}) - C_2(1 - e^{-A_2\|v_r\|})\Big] \tag{2}$$

where μ is the estimated friction coefficient, and C_1, C_2, A_1 and A_2 are the fitting parameters of the model.

1.2 Structure of Paper

The remainder of this paper is organised as follows: Section 2 describes the simulation models used in this research; Section 3 lists the control objectives and describes each controller investigated; Section 4 outlines the important results obtained from simulation of each controller. Preliminary experimental results supporting these simulations are presented in Section 5. Concluding remarks are given in Section 6, and directions for further work are suggested in Section 7.

2 System Modelling

Figure 2 illustrates the control structure used to simulate a two-wheeled robot. The control structure used, particularly the motor models, was developed to closely match the physical platform used to obtain the experimental results presented in Section 5.

The environment input determines the type of friction model used; in this work the environment is time-invariant. The desired robot velocity is $0m/s$. In the

remainder of this section the motor dynamics, platform models and friction models will be described.

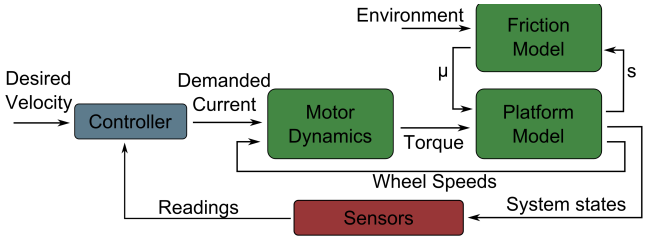

Figure 2: System control diagram

2.1 Motor Modelling

The drive wheel and reaction-wheel motors are run in current control mode, i.e. the motor drivers match the motor coil current to the controller output, altering the phase voltage as necessary. This simplifies control as the controller output corresponds directly to motor torque. The torque available for balancing is also a function of gear train friction, modelled by

$$T_M, T_R = K_t u - K_f \omega \tag{3}$$

where T_{out} is the torque applied to the wheel or IB, K_t is the torque constant of the motor, u is the current demanded by the controller, K_f is the friction constant and ω is the wheel angular velocity. Utilizing current control introduces a delay between the controller output and the motor coil current, however this delay is assumed to be negligible.

2.2 Platform Modelling

To derive a dynamic model of the robot accounting for slip effects, a derivation assuming no slip was used as a starting point. Both models are presented here for comparison. For both derivations, it is assumed that the ground and tires are non-deformable i.e. there is a single point of contact for each wheel.

Both derivations begin with force and moment analysis of the IB and wheel section; Figure 3 illustrates the notation used in forming these equations. Note that T_M and T_R, which represent the main drive wheel and reaction-wheel torques respectively, are shown in the direction acting on the wheels. In order to make the system of equations complete, a final equation is required which differs between the no-slip and slip-inclusive derivations.

No-Slip Derivation

The no-slip kinematic constraint Equation (4) is used.

$$\ddot{x} = \ddot{\phi} r \tag{4}$$

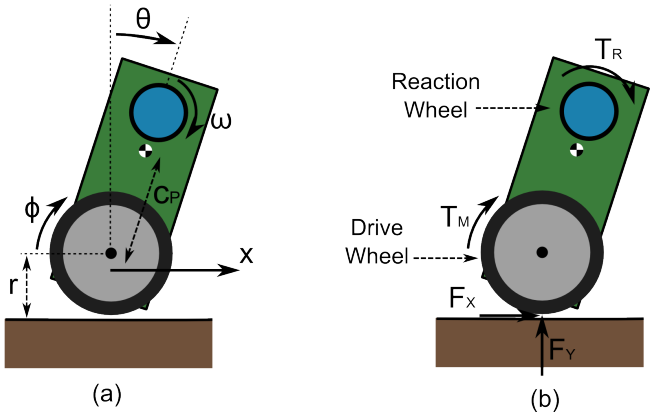

Figure 3: Two-wheeled robot notation (a) Kinematics (b) Forces

Solving the system of equations, we find Equations (5) and (6), forming the no-slip dynamic model.

$$\ddot{x} = \frac{1}{d_1}\begin{pmatrix} aI_O\dot{\theta}^2\sin\theta - a^2 g\sin\theta\cos\theta\ldots \\ \ldots + T_M(\frac{I_O}{r} + a\cos\theta) + T_R a\cos\theta \end{pmatrix} \tag{5}$$

$$\ddot{\theta} = \frac{1}{d_1}\begin{pmatrix} -a^2\dot{\theta}^2\sin\theta\cos\theta + am_O g\sin\theta\ldots \\ \ldots - T_M(m_O + \frac{a}{r}\cos\theta) - T_R m_O \end{pmatrix} \tag{6}$$

where

$$d_1 = I_O m_O - a^2\cos^2\theta$$

$$m_O = \frac{I_W}{r^2} + m_W + m_P$$

$$I_O = I_P + m_P c_P^2$$

$$a = m_P c_P^2$$

where m_W and m_P are the wheel section and IB masses respectively, I_W is the wheel rotational inertia about the wheel axle and I_P is the IB rotational inertia about the IB centre of mass.

Slip-Inclusive Derivation

Equation (7) is introduced to relate the normal and friction forces at the wheel-ground contact point by the coefficient of friction.

$$\mu = \frac{F_x}{F_y} \tag{7}$$

The coefficient of friction may change dynamically as a function of the system states and inputs. Solving the new system of equations gives Equations (8), (9) and (10), the slip-inclusive dynamic model.

$$\ddot{x} = \frac{a}{d_2}\begin{pmatrix} (\cos\theta + \mu\sin\theta)(T_M + T_R - ag\sin\theta)\ldots \\ \ldots + I_O\dot{\theta}^2(\sin\theta - \mu\cos\theta) + \mu g m_T I_O \end{pmatrix} \tag{8}$$

$$\ddot{\theta} = \frac{1}{d_2}\begin{pmatrix} (\mu\cos\theta - \sin\theta)(a^2\dot{\theta}^2\cos\theta - agm_T)\dots \\ \dots - m_T(T_M + T_R) \end{pmatrix} \tag{9}$$

$$\ddot{\phi} = \frac{T_M}{I_W} + \frac{r\mu}{I_W}\begin{pmatrix} (gm_T - a\dot{\theta}^2\cos\theta)(a^2 - m_T I_O)\dots \\ \dots - am_T\sin\theta(T_M + T_R) \end{pmatrix} \tag{10}$$

where

$$d_2 = m_T I_O - a^2\cos\theta(\cos\theta + \mu\sin\theta)$$

$$m_T = m_W + m_P$$

Additionally, both models require Equation (11) to describe the reaction-wheel motion, resulting in 3 degrees-of-freedom for the no-slip model and 4 degrees-of-freedom for the slip-inclusive model.

$$\dot{\omega} = \frac{T_R}{I_R} \tag{11}$$

Looking at the no-slip model, we see that the main drive wheel torque has two effects on the system, i.e. mechanisms to achieve stability. The first mechanism is the wheel axle being forced beneath centre of mass of the IB, affecting the tilt angle. The second mechanism is the reaction to the supplied torque itself; these terms match those of the reaction-wheel torque input. This conclusion is important as although the first mechanism of the drive wheel torque can be nullified by insufficient ground friction, the second is independent of friction, as can be seen in the slip-inclusive model equations.

2.3 Friction Modelling

In addition to the no-slip model, two low-friction surfaces are simulated. The first has been tuned to have peak and eventual friction coefficients similar to ice [Gustafsson, 1997], and is modelled by Equation 2, with the following coefficients: $C_1 = 0.3, C_2 = 0.27, A_1 = 2.45, A_2 = 2$, resulting in the wheel slip curve shown in Figure 4. The second low-friction surface investigated is a frictionless surface modelled using $\mu = 0$.

2.4 Sensor Modelling

The effects of sensor characteristics such as noise, biases and time delays have not been investigated. It is assumed that the sensors provide feedback of all relevant system states: $\dot{x}$, θ, $\dot{\theta}$, ω, and $\dot{\phi}$.

2.5 Physical Platform Parameters

The parameter values used in simulation were measured from the physical testing platform, and are tabulated in Table 1.

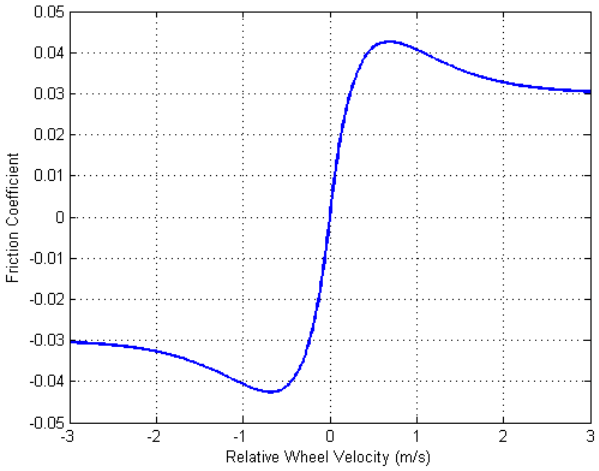

Figure 4: Wheel slip curve of simulated low-friction surface

3 Controller Design

The objective of controller design is robot tilt angle stability. Controller performance will be quantified by the overshoot and settling time of the tilt angle response of the robot, starting from rest with an initial tilt angle of 10°.

3.1 Baseline controller

The first controller investigated is used as the baseline in this study. It is similar to controllers used by other researchers [Grasser *et al.*, 2002; Kim *et al.*, 2005] to achieve TWR stability in no-slip environments, and consequently only the main drive wheel actuators are utilised. In addition to keeping the tilt angle to a minimum, this controller attempts to track the robot velocity to a reference speed input, which compensates for mass imbalances in the robot.

The no-slip dynamic model is linearised about a tilt angle of zero, and linear quadratic regulation (LQR) is used to find optimal gains for the state vector,

$$\underline{x_b} = \left[\int (\dot{x} - v_{ref})\, dt \quad \dot{x} \quad \theta \quad \dot{\theta}\right]^T.$$

The state and input weightings were tuned to provide the shortest tilt angle settling time on a no-slip surface. Figure 5 illustrates the response of this controller, starting at rest from an initial tilt angle of 10°, on three surfaces: constrained no-slip, low-friction and frictionless. The controller response deteriorates with decreasing friction and on frictionless terrain the system is unstable. This failure is the motivation for an improved controller.

3.2 Low-friction controller

The second controller investigated was designed specifically for low-friction surfaces. The slip-inclusive model

Table 1: Parameter values used in simulation

Name	Symbol	Value
Intermediate Body Parameters		
IB mass	m_P	$43kg$
IB rotational inertia	I_P	$0.56kg.m^2$
CoM to wheel axle distance	c_P	$0.2m$
Wheel Section Parameters		
Wheel mass	m_W	$5.54kg$
Wheel rotational inertia	I_W	$0.178kg.m^2$
Wheel radius	r	$0.196m$
Motor torque constant	$K_{t,M}$	$1.5Nm/A$
Motor friction constant	$K_{f,M}$	$1.4Nm/rad.s$
Demanded current limits	$-$	$\pm 5A$
Reaction Wheel Parameters		
RW rotational inertia	I_R	$0.05kg.m^2$
Motor torque constant	$K_{t,R}$	$0.75Nm/A$
Motor friction constant	$K_{f,R}$	$0.7Nm/rad.s$
Demanded current limits	$-$	$\pm 5A$

was linearised about $\theta = 0$ and $\mu = 0$. In such frictionless environments, the forward velocity becomes uncontrollable; hence velocity reference tracking is not available. Instead, this controller tracks wheel slip to zero, providing the robot with greater stability upon returning to surfaces with friction. The controller is tuned using LQR with the state vector,

$$\underline{x_l} = \left[\int \left(\dot{\phi} - \dot{x}/r \right) dt \quad \theta \quad \dot{\theta} \quad \dot{\phi} \right]^T.$$

3.3 Reaction wheel controller

The final controller investigated is similar to the low-friction controller, however, this controller makes use of the reaction-wheel actuator in addition to the main drive wheels. The motivation for this controller is to investigate the potential of the reaction-wheel actuator in this application. This controller is tuned in the same way as the low-friction controller, with ω added to the state vector.

4 Simulation Results

Model simulation was performed using MATLAB and Simulink, under the three friction conditions described.

4.1 No-slip environments

Figure 6 shows the response of each controller in a no-slip environment. All controllers exhibit fast, smooth responses bringing the tilt angle close to zero. The error in tilt angle at the completion of the simulation for the baseline controller is due to the relatively small gain on

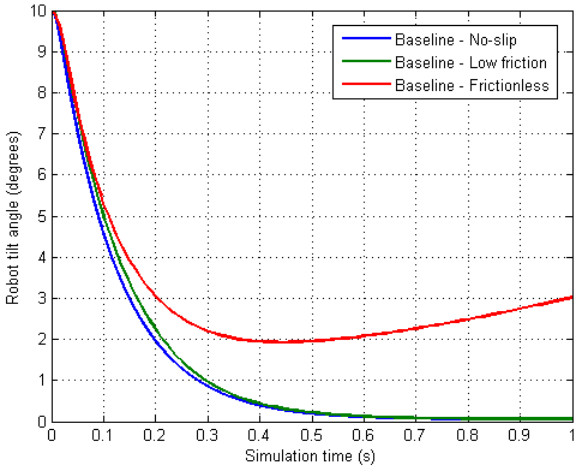

Figure 5: Baseline controller response on various surfaces

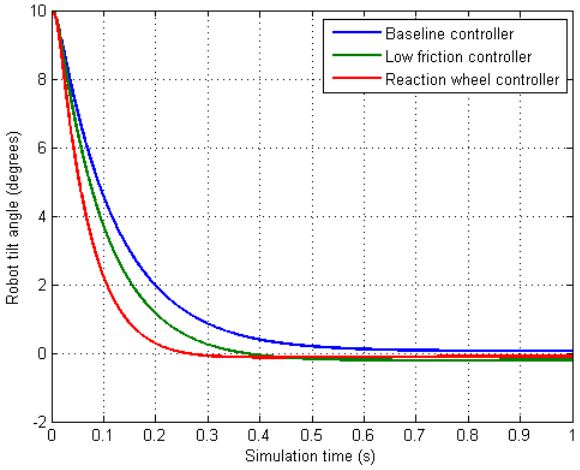

Figure 6: Controller responses on no-slip surface

reference speed; after sufficient time the tilt angle reaches $0°$.

The low-friction controller has a faster settling time than the baseline controller. This is expected to be due two factors. Firstly, the baseline controller also has the velocity tracking objective to satisfy. Secondly, the low-friction controller produces greater actuation to perturbations, as in frictionless environments the main drive wheel torque has less effect on the system than in no-slip environments.

Finally, the reaction-wheel controller exhibits a faster settling time than both other controllers. This is due to the increase in available torque output, as shown in Figure 7. In the initial $0.02s$ both the baseline and low-friction controllers are limited by the main drive wheel torque limits, but the reaction-wheel controller is able to

source an additional $30Nm$ from the reaction-wheel.

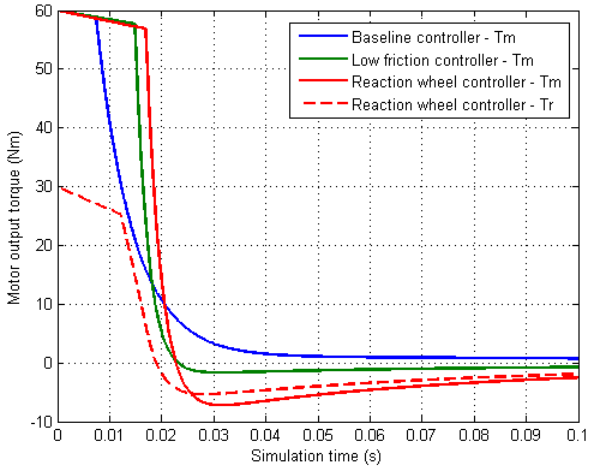

Figure 7: Motor output torques for each controller on a no-slip surface

4.2 Low-friction environments

Figure 8 shows the performance of the three controllers on a low-traction surface. In this situation the advantage of the newer controllers over the baseline is apparent; the tilt angle settling time is significantly improved. The reaction-wheel controller has the fastest settling time, primarily due to the increase in maximum torque output as explained earlier. However, it also shows a significant tilt angle overshoot which may be undesirable.

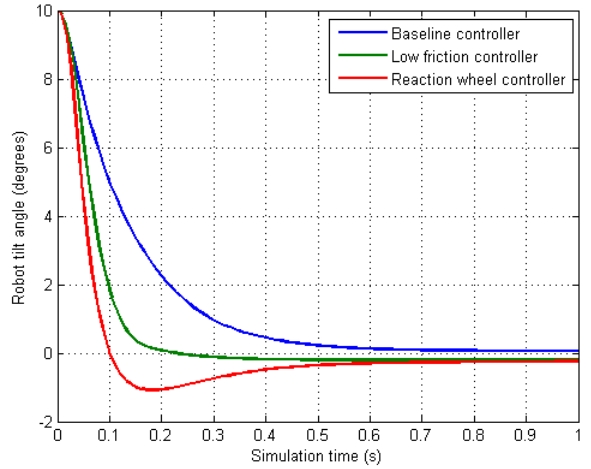

Figure 8: Controller responses on low-traction surface

4.3 Frictionless environments

The controller responses on a frictionless surface are illustrated in Figure 9. In this environment, the baseline controller fails to keep the robot stable, while the low-friction and reaction-wheel controllers succeed, albeit with significant overshoot. Of course, it is not suprising that the latter two controllers achieve stability, as they were tuned specifically for this surface.

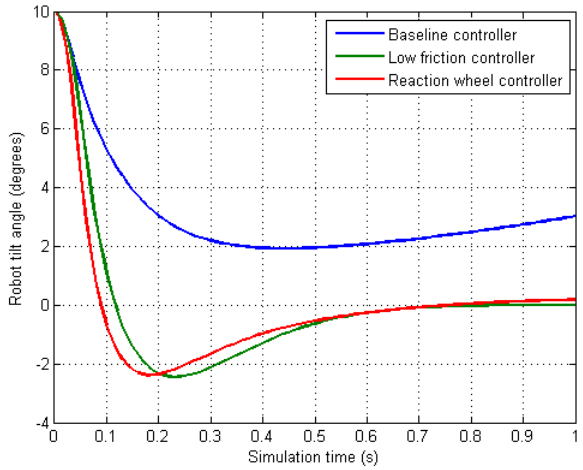

Figure 9: Controller responses on a frictionless surface

5 Experimental Results

Experimental testing was conducted using the TWR pictured in Figure 10, using a sample rate of $50Hz$. The chassis and drive wheels of this robot were taken from a Segway p133 HT. Significant modifications were made to the chassis: structural modifications to raise the centre of gravity above the drive wheel axles, a control computer to facilitate experimental testing, and a reaction wheel motor to investigate the potential improvements of such actuators.

The aim of experimental testing was to validate the simulation results presented. No-slip surface testing was conducted on medium-density-fibre board; no wheel slip was observed on this surface. To approximate an ice-like surface in the laboratory, the robot was placed on Teflon sheets. Unfortunately it was found that the robot tires still had significant traction on this surface. Alternative methods to simulate such a low-traction surface will be considered in future work.

To approximate frictionless surfaces experimentally a bearing was attached to each drive wheel axle. The weight of the TWR was supported by the bearings, lifting the drive wheels above the ground surface as shown in Figure 10, restricting the drive wheels to behave simply as reaction wheels. This configuration has two advantages over other methods of simulating frictionless surfaces, e.g. dynamometers: the rotational inertia of the drive wheels is unchanged, and if the bearings are supported on flat

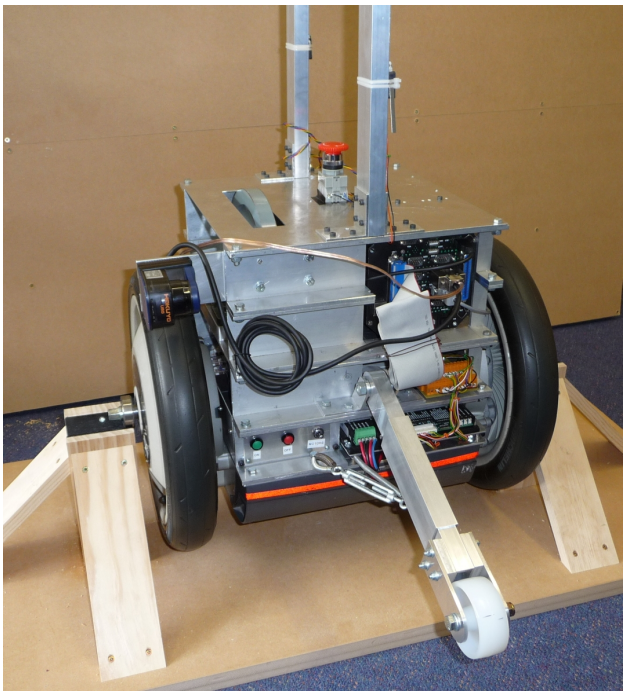

Figure 10: Photograph of TWR in the frictionless surface testing configuration

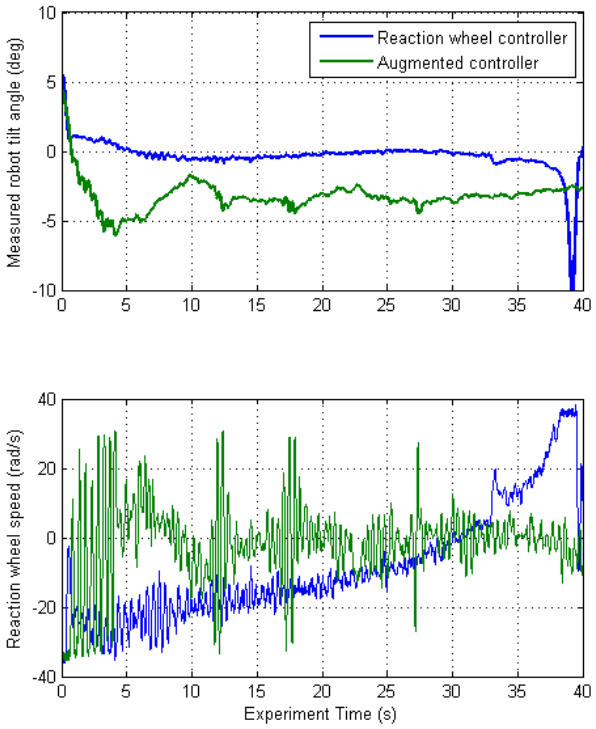

Figure 11: Controller responses to an inital tilt angle of approximately 5° in frictionless surface testing configuration

rails the robot is free to move longitudinally as it would on a true frictionless surface. However, longitudinal motion was restricted in the following test cases.

5.1 Frictionless environments

Using the main drive wheels as reaction wheels was found to be ineffective for balancing. The wheels quickly reached a maximum velocity at which the motor back-EMF voltage matched the supply voltage, thereby preventing the motors from supplying any additional torque. The high gear ratio of 24 in the drive wheels is believed to be the main contributing factor.

The reaction wheel, however, was able to maintain balance in frictionless tests. The reaction wheel controller discussed earlier was used, with gains retuned to accomodate unmodelled effects. However, without the drive wheels, the state vector for the controller is reduced to

$$\underline{x_r} = \begin{bmatrix} \theta & \dot{\theta} & \omega \end{bmatrix}^T.$$

With the controller now lacking any integral component, it was found the robot would eventually fall over due to mass imbalances. To alleviate this problem, the integral of the reaction wheel speed was introduced to the state vector. Figure 11 illustrates the robot tilt angle and reaction wheel speed responses of both controllers to an initial tilt angle of approximately 5°.

It is important to note that the tilt angles measured during these experiments include errors of up to ±1° and mass imbalances of around 3°. Therefore, the true tilt angle at which the robot is balanced is not measured as 0°.

Both controllers are able to bring the robot back to 0°, reaching steady state within 5 and 15 seconds respectively. While the first controller causes the robot to fall after about 38 seconds due to reaction wheel saturation, the second controller is able to keep the robot balanced for much longer intervals e.g. over 10 minutes. Note that the first controller attempts to regulate to 0° tilt angle, while the second controller brings the robot to the correct balanced tilt angle, taking mass imbalances and IMU drift into account. The significant oscillations shown have a period of about 0.4 seconds and are due to the delay between the tilt rate measurement and the reaction wheel motor.

5.2 No-slip environments

An ideal controller would be able to maintain balance on both frictionless and no-slip surfaces, and simulation results indicated the later two controllers could. With the aim of supporting these results experimentally, the response of the augmented controller discussed in the

previous section was tested on the no-slip surface, without gain retuning. Figure 12 illustrates the tilt angle and reaction wheel speed responses in this configuration.

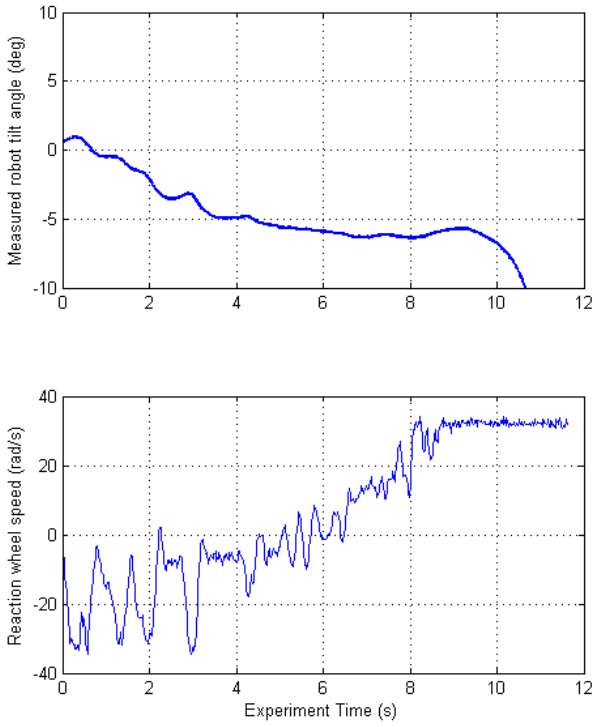

Figure 12: Augmented controller response on the no-slip surface

The controller is unable to keep the robot balanced for longer than 10 seconds, after this time reaction wheel saturation causes failure. Additionally, the period of oscillations in the response is increased, due to the increase in effective inertia of the system - the robot is now pivoting about the wheel-ground contact point, rather than the drive wheel axle. The reaction wheel speed response reflects the one exhibited by the reaction wheel controller on a frictionless surface, which suggests the gains on the reaction wheel needed to be increased. Overall, the increased inertia of the robot in this configuration causes the controller to fail.

The controller was retuned with the objective of balancing on a no-slip surface using the reaction wheel. This was not achieved with the given controller; reaction wheel saturation proved to be a significant problem. Unmodelled tire effects, e.g. assuming the tire-ground contact patch is a single point, are expected to be the main factor.

Due to technical problems, we were unable to test the drive wheels and reaction wheels simultaneously on a no-slip surface. As drive wheel control on no-slip surfaces is a well-studied area, we did not consider the use of the drive wheels experimentally.

6 Conclusions

Two friction conditions were investigated in this paper: one with characteristics similar to ice, and the other frictionless. However, the slip-inclusive TWR dynamic model derived in this work can be applied to a variety of friction models observed in literature, including dynamic friction models.

The two newly developed controllers outperform the baseline reference-tracking controller in simulation. An important conclusion is that while the baseline controller is unstable on a frictionless surface, the newer controllers achieve stability. This result was supported by experimentation: the reaction wheel controller, with a modification to allow for mass imbalances, was able to balance the robot on an approximation of a frictionless surface. However, when the robot was placed on a no-slip surface, the controller failed to keep the robot balanced, due to the increased robot inertia and unmodelled tire effects, which was contrary to the simulation results.

The main drive wheels were found to be ineffective as reaction wheels during experimental testing, due to the high gear ratio.

One benefit of the addition of a reaction-wheel is faster robot stability response; this has been demonstrated in simulation by the reaction-wheel controller. Additionally, the reaction wheel actuator has been shown to successfully balance the robot on frictionless surfaces, where the drive wheels were ineffective.

One final advantage of the reaction-wheel actuator which is expected to be significant, but which has not been demonstrated, is that the effect of the reaction torque is independent of friction, which is known to have a non-linear and unpredictable nature. For this reason, it is expected that balancing in experimental situations upon low-traction terrain will be much smoother when the reaction-wheel is used.

7 Further Work

Robot stability was the objective of controller design in this paper. Other control objectives of interest include disturbance rejectance, robustness to parameter variation, and velocity reference tracking to enable the TWR to follow movement commands. Fulfillment of these objectives is necessary for useful and safe human-interaction.

Friction estimation has been investigated by a number of researchers [Gustafsson, 1997; Kim *et al.*, 2005; Lee *et al.*, 2004]. This technique allows the peak friction coefficient to be predicted before slip occurs, by observing the shape of the wheel slip friction coefficient relationship at low slip values. The ability to predict the peak friction

coefficient would be very useful to a TWR traversing a low-traction surface. TWRs with reaction-wheel actuators will further benefit from friction estimation by gaining the option to utilise only the reaction-wheel when very little traction is predicted.

Acknowledgments

The authors would like to acknowledge the assistance of the Dynamics & Control Group at the University of Auckland, and fellow postgraduate student Zareena Kausar for her input.

References

[Grasser *et al.*, 2002] Felix Grasser, Aldo D'arrigo, Silvio Colombi, Alfred Rufer. JOE: A Mobile, Inverted Pendulum. *IEEE Transactions on Industrial Electronics* 49(1):107--114, February 2002.

[Gustafsson, 1997] Fredrik Gustafsson. Slip-based tire-road friction estimation. *Automatica* 33(6):1087--1099, June 1997.

[Kausar *et al.*, 2010] Zareena Kausar, Karl Stol, and Nitish Patel. Performance Enhancement of a Statically Unstable Two Wheeled Mobile Robot Travesing an uneven surface. In *Proceedings of the 2010 IEEE International Conference on Robotics, Automation and Mechatronics*, pages 156--162, Singapore, June 2010.

[Kim *et al.*, 2005] Yeonhoon Kim, Soo Hyun Kim and Yoon Keun Kwak. Dynamic Analysis of a Nonholonomic Two-Wheeled Inverted Pendulum Robot. *Journal of Intelligent and Robotic Systems*, 44(1):25--46, September 2005.

[Lee *et al.*, 2004] Chankyu Lee, Karl Hedrick, Kyongsu Yi. Real-time slip-based estimation of maximum tire-road friction coefficient. *IEEE/ASME Transactions on Mechatronics* 9(2):454--458, June 2004

[Müller *et al.*, 2003] Steffen Müller, Michael Uchanski, Karl Hedrick. Estimation of the maximum tire-road friction coefficient. *Journal of Dynamic Systems, Measurement, and Control* 125(4):607--617, December 2003

[Nguyen *et al.*, 2004] Hoa G Nguyen, John Morrell, Katherine Mullens, Aaron Burmeister, Susan Miles, Nathan Farrington, Kari Thomas, and Douglas W. Gage. Segway Robotic Mobility Platform. In *Mobile Robots XVII, Proceedings of the SPIE, Volume 5609*, pages 207--220, Philadelphia, PA, December 2004.

[Pacejka *et al.*, 1987] Hans B Pacejka, Egbert Bakker, Lars Nyborg. Tyre modelling for use in vehicle dynamics studies. *SAE paper* 870421, January 1987

[Shimada and Hatakeyama, 2008] Akira Shimada and Naoya Hatakeyama. Movement control of two-wheeled inverted pendulum robots considering robustness. In *Proceedings of the SICE Annual Conference*, pages 3361--3365, Tokyo, 2008.

[Ward and Iagnemma, 2008] Chris C Ward, Karl Iagnemma. A Dynamic-Model-Based Wheel Slip Detection for Mobile Robots on Outdoor Terrain. In *IEEE Transactions on Robotics* 24(4):821--831, August 2008.

[Wong, 1978] Jo Yung Wong. *Theory of Ground Vehicles*, pages 13--21. Wiley, New York, 1978.